THE PUBLISHING HOUSE
OF THE ROMANIAN ACADEMY

PROCEEDINGS OF THE ROMANIAN ACADEMY, Series A,
Volume 7, Number 2/2006, pp. 000-000

THIN HYDROFOIL CASCADE DESIGN AND NUMERICAL FLOW ANALYSIS PART I - DESIGN

Romeo SUSAN-RESIGA[†‡], Sebastian MUNTEAN[‡], Sandor BERNAD[‡], Teodora FRUNZĂ[†], Daniel BALINT[†]

[†] "Politehnica" University of Timişoara, Bd. Mihai Viteazu 1, RO-300222, Timişoara
[‡] Romanian Academy - Timişoara Branch, Center for Advanced Research in Engineering Sciences, Bd. Mihai Viteazu 24, RO-300222, Timişoara
Corresponding author: Romeo SUSAN-RESIGA, "Politehnica" University of Timişoara, Bd. Mihai Viteazu 1, RO-300222, Timişoara, phone: ++40-256-403692; fax: ++40-256-403700, e-mail: resiga@mh.mec.upt.ro

This two-part paper presents the development and implementation of robust, efficient and accurate numerical algorithms for hydrofoil cascade design, analysis and optimization. First, we review the analytical approach for designing thin hydrofoil cascades with a given loading distribution. The hydrofoil has zero incidence at leading edge, and satisfies the Kutta-Joukowsky condition at trailing edge. A Hermite representation, with continuous derivatives, is used for the hydrofoil shape and the nonlinear integral equation for the hydrofoil design is solved iteratively. The non-linear integral equations are solved iteratively, and the convergence rate is investigated. Two turbine cascade examples are presented, emphasizing the departure of the thin hydrofoil shape from the prescribed pitch-averaged streamline.

Keywords: hydrodynamics, hydrofoil cascade design

1. INTRODUCTION

The cascade model is defined as an infinite row of equidistant similar airfoil-shaped bodies, and plays a central role in turbomachines design, analysis and optimization. As pointed by Gostelow [5], the cascade is merely a model. In fluid mechanics the process of modelling is one of physical and mathematical simplification and is intended to result in a rationalization and deeper understanding of the flow field behaviour. As a result, the cascade flow analysis benefits from a large body of literature dealing with both experimental as well as theoretical studies. The Timişoara School of Turbomachinery Hydrodynamics was particularly focused on experimental investigation of linear [2] and radial [6] cascades, as well as on developing analytical [10] and numerical [4] methods for cascade flow computation. Both energetical and cavitational [1] characteristics of the hydrofoil cascades were investigated in order to provide the required information for improving the hydraulic machines design.

The classical methods for cascade flow analysis have been summarized more than two decades ago in monographies such as [5] and [13], and experimental results have been collected in catalogs such as [11] and [3]. More recently, the focus has switched from using available aero- hydrofoil shapes and data toward numerical design and optimization such that carefully chosen flow specifications are met directly in the design stage. The main idea is to prescribe either the flow on the hydrofoil shape or the pitchwise averaged flow and compute the corresponding streamlined body shapes.

Zangeneh [12] briefly reviews the inverse design methods available for two-dimensional cascades. Ideally one would like to prescribe the pressure or velocity distribution on the pressure and suction surfaces so that the blades are designed with optimized boundary layers. However, this type of design specification has no control over blade thickness and could result in an ill-posed problem. For example, Lighthill found that it is impossible to specify the velocity distribution on the pressure and suction surfaces together with the upstream and downstream boundary conditions. As a result some authors prefer to prescribe the velocity (or pressure) distribution on the suction surface and the thickness distribution, whereas others have proposed methods in which the blade pressure loading is prescribed together with a thickness distribution. Lewis [9]

Recommended by Ioan ANTON, member of the Romanian Academy

also considers that attempting to specify a prescribed velocity distribution (and therefore pressure distribution) on both suction and pressure surfaces at best may lead to unsuitable profile thickness distribution. As a result, the prescribed velocity distribution is limited to the more aerodynamically sensitive upper surface only, but a profile thickness is also prescribed. This inverse method is then used to design the camber line shape required to achieve the desired velocity distribution on the suction side. The velocity distribution on the pressure side is simply accepted to adjust freely to whatever it will.

A particularly important requirement when designing a cascade is to insure the so-called "shock-free" inflow condition. This terminology is a little unfortunate since it has nothing to do with the shock waves caused by compressibility effects in high speed flow. It is instead frequently used to refer to the particular inlet angle for which the leading edge stagnation point is located precisely on the end of the profile camber line. For greater or smaller inlet angles the stagnation point will move instead onto the pressure or suction surfaces, respectively. Shock-free inlet flow thus ensures the smoothest entry conditions into the cascade and is thus likely to be close to the minimum loss situation. However, the shock-free inlet angle may not necessarily coincide exactly with that for minimum loss, which will usually be one or two degree greater [9]. The methodology introduced by Hawthorne et al. [7] directly enforces the shock-free condition at the leading edge of thin hydrofoil cascades.

This two-part paper presents the authors ongoing efforts to develop a robust and efficient numerical methodology, and the associated expert software, for analysis, design and optimization of hydrofoil cascades. The main goal is to automatically optimize the hydrofoil shape for best efficiency as well as for best cavitational characteristics. In Section 2 we review the method for designing thin blade cascades starting from a prescribed flow deflection schedule. An original numerical method is developed for computing the thin blade shape, and two turbine cascade examples are presented in Section 3. The paper conclusions are summarized in Section 4.

2. THIN HYDROFOIL CASCADE DESIGN

Hawthorne et al. [7] developed a quasi-analytical method for designing two-dimensional highly loaded cascades. The fluid is assumed to be incompressible and inviscid and the blades are assumed to have zero thickness and incidence so that there are no stagnation points at the leading edges. In analysing the potential flow through the cascade, one assumes that the thin blades may be represented by bound vortices of strength $\gamma(x)$ distributed along camber lines given by $y - f(x) = 0, \pm s, \pm 2s, \cdots$, where s is the blade spacing, or pitch, Fig. 1. All lengths are made dimensionless by the cascade axial extent. The goal of the cascade design is to find the camberline shape $f(x)$ given the flow direction far upstream, α_1, and downstream, α_2, the spacing s, as well as the vortex strength distribution $\gamma(x)$.

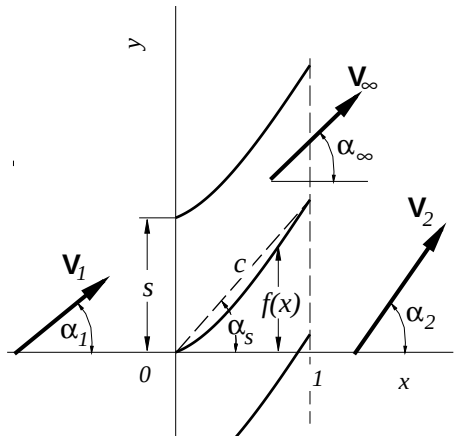

Fig. 1. Thin hydrofoil cascade notations.

When employing a quasi three-dimensional approach for turbomachinery design and analysis, the axial symmetry assumption implies the use of pitch-averaged velocity vector,

$$\bar{\mathbf{V}}(x) = \frac{1}{s}\int_0^s \mathbf{V}(x,y)\,\mathrm{d}y\,. \tag{1}$$

If the velocities upstream and downstream the cascade are $\bar{\mathbf{V}}_1$ and $\bar{\mathbf{V}}_2$, respectively, we have

$$\bar{V}_{x1} = \bar{V}_{x2} = \bar{V}_x\,,\ \text{and}\ \bar{V}_{y2} - \bar{V}_{y1} = \frac{1}{s}\int_0^1 \gamma(x)\,\mathrm{d}x\,. \tag{2}$$

Obviously, for blades with zero thickness the pitchwise mean value of the axial velocity remains constant within the bladed region as well. We can also introduce a pitchwise averaged boundary vorticity,

$$\bar{\gamma}(x) \equiv \frac{\gamma(x)}{s} = \frac{\mathrm{d}\bar{V}_y}{\mathrm{d}x}, \tag{3}$$

and the pitch-averaged tangential velocity can be written as

$$\bar{V}_y(x) = \bar{V}_{y1} + \int_0^x \bar{\gamma}(t)\mathrm{d}t . \tag{4}$$

One can see from (4) that for cascade design we can alternatively provide the $\bar{V}_y$ schedule instead of $\bar{\gamma}$. An average streamline, starting at origin, can also be found as,

$$\bar{f}(x) = \int_0^x \bar{V}_y(t)\mathrm{d}t . \tag{5}$$

The above average streamline, $\bar{f}(x)$, does not correspond to any actual streamline in a finite pitch cascade. However, it might be seen as the representative streamline in the limit $s \to 0$, or for infinitely dense csacade.

In conventional cascade theory, the velocity field $\mathbf{V}(x,y)$ is written as the superposition of the vector mean of the upstream and downstream flow, $\mathbf{V}_\infty \equiv (\mathbf{V}_1 + \mathbf{V}_2)/2$, and the velocity $\hat{\mathbf{V}}(x,y)$ induced by the vortices,

$$\mathbf{V}(x,y) = \mathbf{e}_x \bar{V}_x + \mathbf{e}_y \frac{\bar{V}_{y1} + \bar{V}_{y2}}{2} + \hat{\mathbf{V}}(x,y), \tag{6}$$

where $\mathbf{e}_x$ and $\mathbf{e}_y$ are unit vectors in x- and y-direction, respectively. The vorticity induced velocity can be written using the Biot-Savart approach, [7],

$$\hat{V}_x(x,y) - i\hat{V}_y(x,y) = -\frac{i}{2}\int_0^1 \bar{\gamma}(t) \frac{\sinh\frac{2\pi}{s}(x-t) - i\sin\frac{2\pi}{s}\left[y - f(t)\right]}{\cosh\frac{2\pi}{s}(x-t) - \cos\frac{2\pi}{s}\left[y - f(t)\right]}\mathrm{d}t . \tag{7}$$

On the blade, the normal velocity must vanish. The normal direction on the blade is given by the vector $\nabla(y - f(x)) = -\mathbf{e}_x f'(x) + \mathbf{e}_y$. Using (6) and (7), the condition of flow tangency on the blade can be written as

$$-f'(x)\bar{V}_x + \frac{\bar{V}_{y1} + \bar{V}_{y2}}{2} - f'(x)\hat{V}_x(x, f(x)) + \hat{V}_y(x, f(x)) = 0, \tag{8}$$

leading to the following integral equation for the camberline shape,

$$\frac{\mathrm{d}f}{\mathrm{d}x}(x) = \frac{1}{2}\left(\frac{\bar{V}_{y1}}{\bar{V}_x} + \frac{\bar{V}_{y2}}{\bar{V}_x}\right) + \frac{1}{\bar{V}_x}\int_0^1 \frac{\bar{\gamma}(t)}{2} \frac{\sinh\frac{2\pi}{s}(x-t) + f'(x)\sin\frac{2\pi}{s}\left[f(x) - f(t)\right]}{\cosh\frac{2\pi}{s}(x-t) - \cos\frac{2\pi}{s}\left[f(x) - f(t)\right]}\mathrm{d}t . \tag{9}$$

By writing the integrand in (9) as

$$\frac{\bar{\gamma}(t)}{2}\frac{s}{2\pi}\frac{\mathrm{d}}{\mathrm{d}x}\ln\left\{\cosh\frac{2\pi}{s}(x-t) - \cos\frac{2\pi}{s}\left[f(x) - f(t)\right]\right\},$$

we can integrate (9). If $f = 0$ at the leading edge $x = 0$, i.e. the camberline starts at the origin, we obtain

$$f(x)=\frac{x}{2}\left(\frac{\bar{V}_{y1}}{\bar{V}_x}+\frac{\bar{V}_{y2}}{\bar{V}_x}\right)+\frac{s}{4\pi}\int_0^1\frac{\bar{\gamma}(t)}{\bar{V}_x}\ln\left\{\frac{\cosh\frac{2\pi}{s}(x-t)-\cos\frac{2\pi}{s}\left[f(x)-f(t)\right]}{\cosh\frac{2\pi}{s}t-\cos\frac{2\pi}{s}f(t)}\right\}\mathrm{d}t \tag{10}$$

The determination of the blade profile $f(x)$ requires the integration of equations (9) and (10), each of which has a singularity at $t=x$. As $t\to x$, we have $f(x)-f(t)\to(x-t)f'(x)$ and we can separate the integrand singularities. With $\bar{V}_x=1$, we can rewrite (9) as,

$$\frac{\mathrm{d}f}{\mathrm{d}x}(x)=\frac{\tan\alpha_1+\tan\alpha_2}{2}+\int_0^1 F_1(x,t)\mathrm{d}t+\frac{s\bar{\gamma}(x)}{2\pi}\ln\frac{x}{1-x}, \tag{11a}$$

where $$F_1(x,t)=\frac{\bar{\gamma}(t)}{2}\frac{\sinh\frac{2\pi}{s}(x-t)+f'(x)\sin\frac{2\pi}{s}\left[f(x)-f(t)\right]}{\cosh\frac{2\pi}{s}(x-t)-\cos\frac{2\pi}{s}\left[f(x)-f(t)\right]}-\frac{s\bar{\gamma}(x)}{2\pi}\frac{1}{x-t}. \tag{11b}$$

Now the integrand F_1 vanishes as $t\to x$ and the integral can be performed with standard quadrature rules. The last term in the right-hand side of (11a) is the Cauchy principal value of the singularity integral. The same approach can be used to remove the singularity in (10),

$$f(x)=x\frac{\tan\alpha_1+\tan\alpha_2}{2}+\int_0^1 F_2(x,t)\mathrm{d}t+\frac{s\bar{\gamma}(x)}{2\pi}\left[\ln\left(\frac{2\pi}{s}\right)+\frac{1}{2}\ln\left(\frac{1+f'^2(x)}{2}\right)+x\ln x+(1-x)\ln(1-x)-1\right] \tag{12a}$$

$$F_2(x,t)=\frac{s\bar{\gamma}(t)}{4\pi}\ln\left\{\frac{\cosh\frac{2\pi}{s}(x-t)-\cos\frac{2\pi}{s}\left[f(x)-f(t)\right]}{\cosh\frac{2\pi}{s}t-\cos\frac{2\pi}{s}f(t)}\right\}-\frac{s\bar{\gamma}(x)}{4\pi}\ln\left\{\left[\frac{2\pi}{s}(x-t)\right]^2\frac{1+f'^2(x)}{2}\right\} \tag{12b}$$

In order to solve the equations (11) and (12), we assume a first guess for the unknown function $f(x)$ and its derivative $f'(x)$, and evaluate the right-hand sides. A suitable first guess is provided by the average streamline (5). The new values for $f(x)$ and $f'(x)$ are further used to evaluate again the right-hand sides in (11a) and (12a), and the iterative process continues until the solution change from one iteration to the next one is smaller than a given threshold.

Since the integrals of F_1 and F_2 cannot be evaluated analytically, we consider a discrete representation of the unknown function. First, a set of points $0=x_1<x_2<\ldots<x_{n+1}=1$ are considered on the unit interval. Our goal is to find the function values $f_1\equiv f(x_1), f_2\equiv f(x_2),\ldots,f_{n+1}\equiv f(x_{n+1})$, as well as the function derivatives $f'_1\equiv f'(x_1), f'_2\equiv f'(x_2),\ldots,f'_{n+1}\equiv f'(x_{n+1})$ using the above iterative method. The function approximation f^h is restricted on each sub-interval $[x_i,x_{i+1}]$ to a cubic polynomial, thus allowing a continuously differentiable approximation $f^h\in C^1$. For notational simplicity, we write x_1 and x_2 in place of x_i and x_{i+1}, respectively. On a subinterval f^h may be written as [8]

$$
\begin{aligned}
&f^h(t) = N_1(t) f_1 + N_3(t) f_2 + N_2(t) f'_1 + N_4(t) f'_2, \\
&N_1(t) = \frac{(x_2 - t)^2 \left[h + 2(t - x_1)\right]}{h^3}, \; N_2(t) = \frac{(t - x_1)(t - x_2)^2}{h^2}, \\
&N_3(t) = \frac{(t - x_1)^2 \left[h + 2(x_2 - t)\right]}{h^3}, \; N_4(t) = \frac{(t - x_1)^2 (t - x_2)}{h^2}, \\
&\text{where } x_1 \le t \le x_2, \text{ and } h = x_2 - x_1.
\end{aligned} \tag{13}
$$

This piecewise cubic approximation for $f(t)$ is used to evaluate $F_1(x,t)$ and $F_2(x,t)$, respectively, at quadrature points. There is no need for an approximation of f' on the sub-intervals. Regular quadrature rules can be employed, since neither $F_1(x,t)$ nor $F_2(x,t)$ have singularities as $t \to x$.

Once the camberline shape $f(x)$ computed, one can compute the velocity field. It is convenient to re-write the velocity vector, $\mathbf{V}$, as the sum of the pitch averaged velocity $\bar{\mathbf{V}}$ and an y-periodic velocity $\tilde{\mathbf{V}}$,

$$
\mathbf{V}(x,y) = \bar{\mathbf{V}}(x) + \tilde{\mathbf{V}}(x,y), \text{ where}
$$

$$
\tilde{V}_x(x,y) = \hat{V}_x(x,y) \text{ and } \tilde{V}_y(x,y) = \frac{\bar{V}_{y1} + \bar{V}_{y2}}{2} - \bar{V}_y(x) + \hat{V}_y(x,y) \tag{14}
$$

Using the identity

$$
\frac{\bar{V}_{y1} + \bar{V}_{y2}}{2} - \bar{V}_y(x) = -\int_0^1 \frac{\bar{\gamma}(t)}{2} \operatorname{sgn}(x - t) \mathrm{d}t,
$$

as well as (7), we have the y-periodic velocity components

$$
\tilde{V}_x(x,y) = -\int_0^1 \frac{\bar{\gamma}(t)}{2} \frac{\sin \frac{2\pi}{s}\left[y - f(t)\right]}{\cosh \frac{2\pi}{s}(x - t) - \cos \frac{2\pi}{s}\left[y - f(t)\right]} \mathrm{d}t \tag{15a}
$$

$$
\tilde{V}_y(x,y) = \int_0^1 \frac{\bar{\gamma}(t)}{2} \left[\frac{\sinh \frac{2\pi}{\mathrm{s}}(x - t)}{\cosh \frac{2\pi}{\mathrm{s}}(x - t) - \cos \frac{2\pi}{\mathrm{s}}\left[y - f(t)\right]} - \operatorname{sgn}(x - t) \right] \mathrm{d}t \tag{15b}
$$

For $y \to f(x)$ we obtain the vector average of the velocity on the upper and lower sides of the thin hydrofoil, $\mathbf{V}_{\mathrm{bl}}(x) \equiv \mathbf{V}(x, f(x))$. The magnitude of the average velocity on the blade can be obtained by taking the scalar product with the tangent unit vector,

$$
\begin{aligned}
V_{\mathrm{bl}}(x) &= \frac{V_{\mathrm{bl}}^{\mathrm{lo}}(x) + V_{\mathrm{bl}}^{\mathrm{up}}(x)}{2} = \mathbf{V}_{\mathrm{bl}}(x) \cdot \boldsymbol{\tau}(x) = \frac{\bar{V}_x + f'(x)\bar{V}_y(x)}{\sqrt{1 + f'^2(x)}} + \frac{1}{\sqrt{1 + f'^2(x)}} \times \\
&\int_0^1 \frac{\bar{\gamma}(t)}{2} \left[\frac{f'(x) \sinh \frac{2\pi}{s}(x - t) - \sin \frac{2\pi}{s}\left[f(x) - f(t)\right]}{\cosh \frac{2\pi}{s}(x - t) - \cos \frac{2\pi}{s}\left[f(x) - f(t)\right]} - f'(x) \operatorname{sgn}(x - t) \right] \mathrm{d}t
\end{aligned} \tag{16}
$$

Note that the integrand vanishes as $t \to x$, thus we have a regular integral.

In addition to the average velocity (16), we can write the velocity jump using the elementary circulation as $\gamma(x)\mathrm{d}x = \left(V_{\mathrm{bl}}^{\mathrm{lo}} - V_{\mathrm{bl}}^{\mathrm{up}}\right)\mathrm{d}l$, where the circulation is positive counterclockwise. As a result, the velocity jump from the lower to the upper side of the thin foil is

$$V_{\mathrm{bl}}^{\mathrm{lo}}(x)-V_{\mathrm{bl}}^{\mathrm{up}}(x)=\gamma(x)\frac{\mathrm{d}x}{\mathrm{d}l}=\frac{\gamma(x)}{\sqrt{1+f'^2(x)}}. \tag{17}$$

Equations (16) and (17) give now the velocity magnitude on the foil lower and upper sides as,

$$V_{\mathrm{bl}}^{\mathrm{lo}}(x)=V_{\mathrm{bl}}(x)+\frac{1}{2}\frac{s\bar{\gamma}(x)}{\sqrt{1+f'^2(x)}} \quad \text{and} \quad V_{\mathrm{bl}}^{\mathrm{up}}(x)=V_{\mathrm{bl}}(x)-\frac{1}{2}\frac{s\bar{\gamma}(x)}{\sqrt{1+f'^2(x)}}. \tag{18}$$

The pressure follows from Bernoulli's theorem. The pressure coefficient is defined with respect to the upstream conditions,

$$c_p=\frac{p-p_1}{\frac{1}{2}\rho\bar{V}_1^2}=1-\left(\frac{V}{\bar{V}_x}\right)^2\cos^2\alpha_1. \tag{19}$$

3. TURBINE CASCADE DESIGN EXAMPLE

Let us consider an example for the cascade design method presented in Section 2. The key ingredient is the vortex strenght distribution function, which is taken here of the form:

$$\bar{\gamma}(x)=(\tan\alpha_2-\tan\alpha_1)\frac{15}{4}\sqrt{x}(1-x). \tag{20a}$$

This function is in agreement with usual considerations concerning hydrofoils currently used in hydraulic machinery blading. One can immediately see that $\sqrt{x}(1-x)$ vanishes at both leading edge and trailing edge, thus providing a shock-free flow and complying with the Kutta-Joukowsky condition, respectively. The integral of the distribution function is $\int_0^1(15/4)\sqrt{x}(1-x)\mathrm{d}x=1$, as required by Eq. (4). Finally, the maximum of the distribution function is reached at $x=1/3$, leading to a larger hydrofoil loading in the front half of the chordlength in comparison to the rear half. Of course, (20a) is not the only choice available, and in practice one should use a parametric vortex strength distribution to provide the required flexibility for optimization studies. However, the present paper is aimed at developing, validating and assessing the accuracy of design and numerical analysis methods to be further used for cascade hydrodynamics studies.

The pitch-averaged tangential velocity can be computed from (4),

$$\frac{\bar{V}_y(x)}{\bar{V}_x}=\tan\alpha_1+(\tan\alpha_2-\tan\alpha_1)\frac{x\sqrt{x}}{2}(-3x+5). \tag{20b}$$

The average streamline that originates at the origin is, according to (5),

$$\bar{f}(x)=x\left[\tan\alpha_1+(\tan\alpha_2-\tan\alpha_1)x\sqrt{x}\left(-\frac{3}{7}x+1\right)\right] \tag{20c}$$

Figure 2 shows the vortex strength (20a), Fig. 2a, tangential velocity (20b), Fig. 2b, and an average streamline (20c), dashed line in Fig. 2c, for a turbine cascade with inlet/outlet angles $\alpha_1=35^\circ$ and $\alpha_2=55^\circ$.

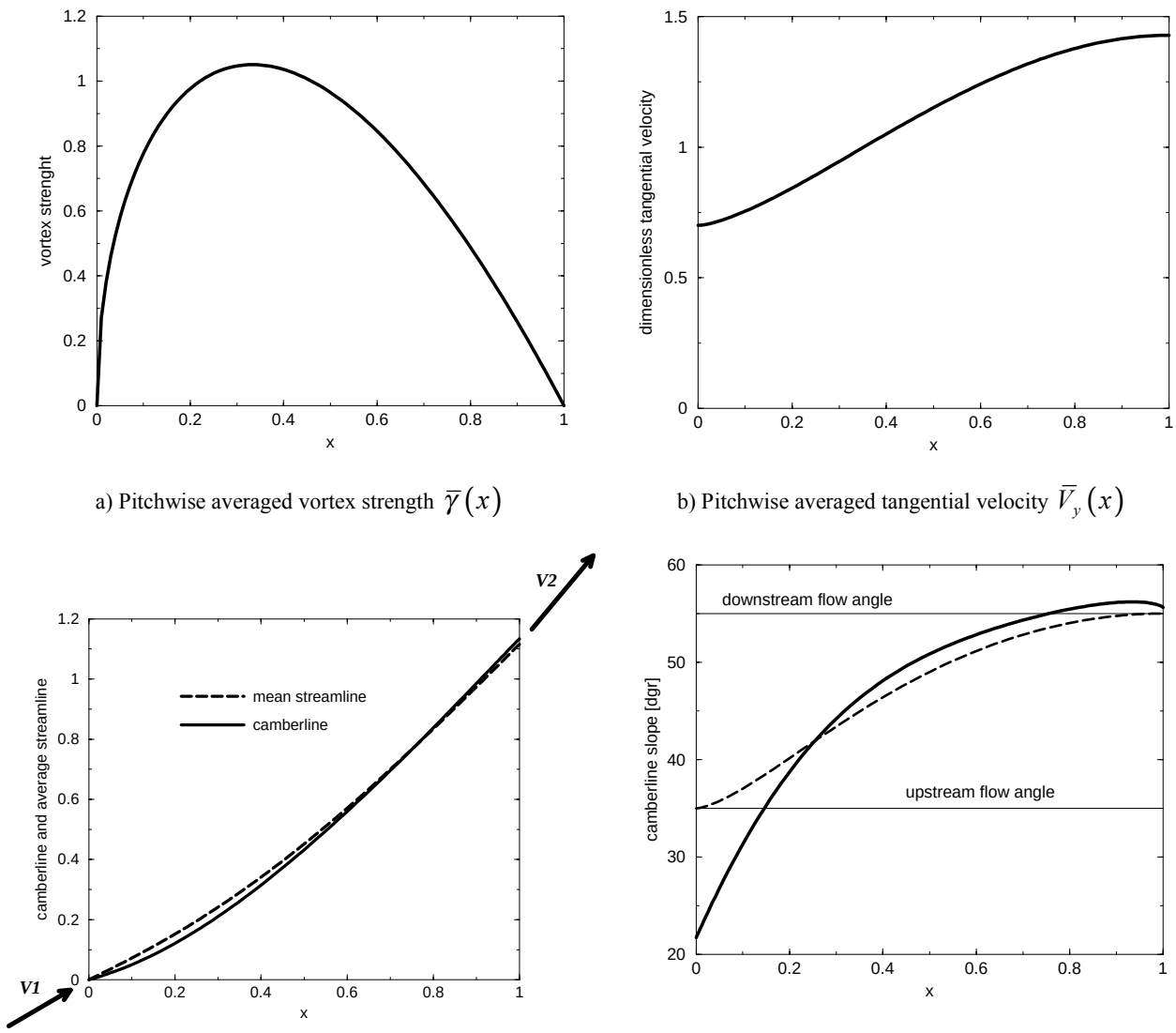

a) Pitchwise averaged vortex strength $\bar{\gamma}(x)$

b) Pitchwise averaged tangential velocity $\bar{V}_y(x)$

c) Mean streamline $\bar{f}(x)$ and camberline $f(x)$.

d) Camberline slope $\arctan(f'(x))$.

Fig. 2. Data for the design of a turbine cascade with $\alpha_1 = 35^\circ$ and $\alpha_2 = 55^\circ$, and the computed camberline for cascade pitch $s = 1$.

The primary design data is $\bar{\gamma}(x)$, but alternatively one could specify the tangential velocity schedule $\bar{V}_y(x)$. The mean streamline $\bar{f}(x)$, shown with dashed line in Fig. 2c, does not depend on the cascade pitch, but the camberline shape, $f(x)$, does. As a result, in addition to the above flow schedule, we need to specify the cascade pitch, s. Since the thin blade shape (camberline) is not know yet, the blade spacing is made dimensionless by the cascade axial extent since we do not know apriori the blade chordlenght. For the first numerical example we have considered a cascade with $s = 1$. The computed camberline is shown Fig. 2c with solid line. Once the camberline known by solving (9) and (10), we can compute its chordline length, leading to the pitch/chord ratio of $s/c = 0.6614532$. The stagger angle, i.e. the angle between the chordline and the axial direction, is $\alpha_s = 48.59^\circ$. Although the difference between the camberline and the average streamline might seem rather small from Fig. 2c, one can see that the difference in slope is quite large, particularly near the leading edge. Fig 2d shows that the camberline direction at leading edge should be 21.7°, quite different from the far upstream flow angle $\alpha_1 = 35^\circ$, in order to obtain zero incidence and shock-free flow. The angle of attack, i.e. the angle between the chordline and the upstream/downstream

vector average velocity $\mathbf{V}_\infty \equiv (\mathbf{V}_1 + \mathbf{V}_2)/2$, is $\alpha_s - \alpha_\infty = 48.59^\circ - 46.78^\circ = 1.81^\circ$. Near the trailing edge the camberline angle is sligthly larger than the downstream flow angle $\alpha_2 = 55^\circ$. An interesting feature is the reverse curvature near the trailing edge, as noted by Hawthorne et al. [7] as well.

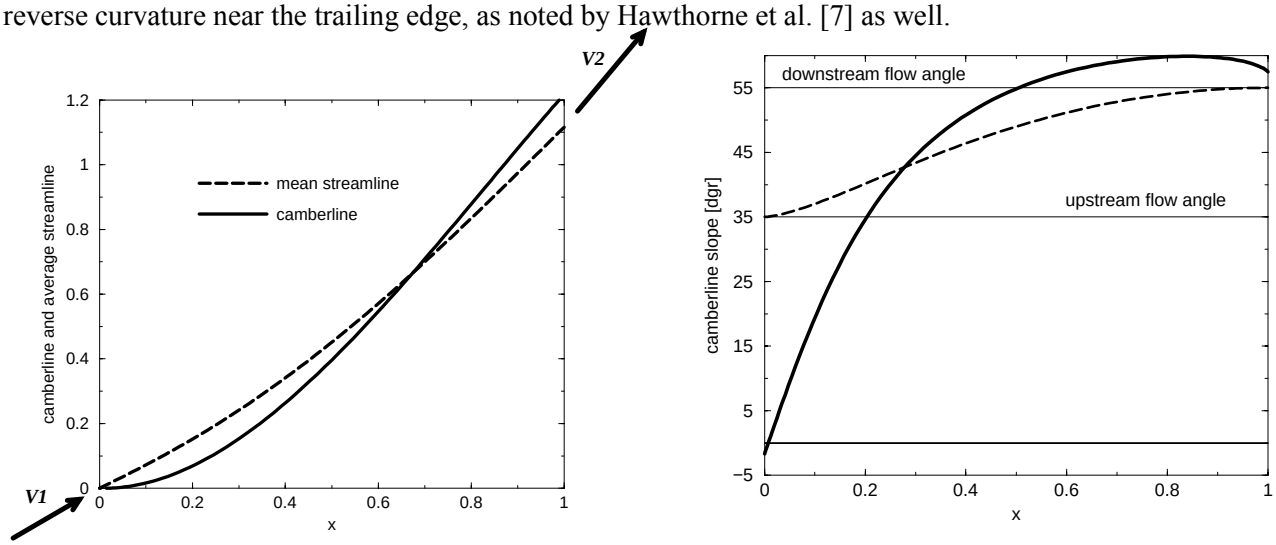

a) Mean streamline $\bar{f}(x)$ and camberline $f(x)$.

b) Camberline slope $\arctan(f'(x))$.

Fig. 3. Turbine cascade with $\alpha_1 = 35^\circ$ and $\alpha_2 = 55^\circ$, and pitch $s = 2$ (pitch/chord ratio $s/c = 1.270120$).

When the cascade pitch is increased to $s = 2$ the blade loading increases and the camberline departure from the mean streamline gets larger, as shown in Fig. 3a. This cascade has a pitch/chord ratio $s/c = 1.270120$ and a stagger angle $\alpha_s = 50.5756^\circ$. The corresponding angle of attack is $\alpha_s - \alpha_\infty = 50.58^\circ - 46.78^\circ = 3.8^\circ$. Figure 3b shows that the camberline is practically aligned with the axial direction at the leading edge, where the camberline angle is -1.7°. At trailing edge the camberline slope 57.47° is larger than the downstream flow angle $\alpha_2 = 55^\circ$, and due to the reverse curvature near the trailing edge the maximum camberline angle is 59.88° at $x = 0.8423$.

Since solving the non-linear integral equation requires an iterative algorithm, we also examine the rate of convergence. The change in the camberline shape at the current iteration m from the previous one $m-1$ is quantified as,

$$\varepsilon^{(m)} = \sqrt{\frac{\sum_{i=1}^{n+1}\left(f_i^m - f_i^{m-1}\right)^2}{n+1}}$$

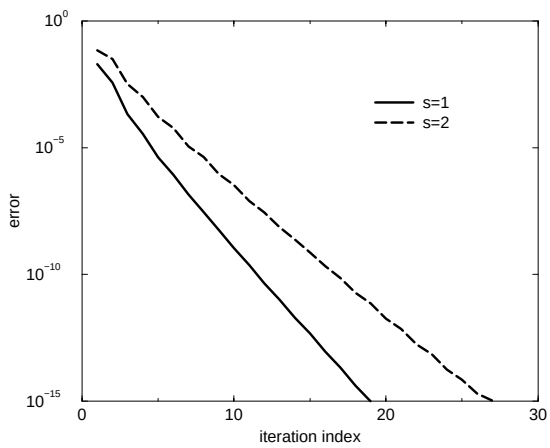

Fig. 4. Convergence of the iterative design algorithm.

One can see from Fig. 4 that the iterative algorithm for solving the nonlinear integral equation displays a linear convergence. However, the convergence rate decreases as the cascade pitch increases.

For future developments of the cascade design algorithm, for example to include a blade thickness distribution, an alternative to equation (10) must be found. Indeed, when deriving (10) we have used the particular form for the integrand in (9). However, this is no longer the case when a thickness distribution is added via a dipol distribution on the camberline. In this case, Eq. (10) should be replaced by a numerical technique to reconstruct the camberline $f(x)$ when $\mathrm{d}f/\mathrm{d}x$ is known from (9). A good candidate for the reconstruction procedure is a cubic spline representation for $f(x)$. Using the function representation (13), we have to impose the continuity of the second derivative at the nodes. In doing so, for each interior node $i = 2\ldots n$ we obtain

$$-\frac{1}{h_{i-1}^2} f_{i-1} + \left(\frac{1}{h_{i-1}^2} - \frac{1}{h_i^2} \right) f_i + \frac{1}{h_i^2} f_{i+1} = \frac{1}{3} \left(\frac{1}{h_{i-1}} f'_{i-1} + 2 \left(\frac{1}{h_{i-1}} + \frac{1}{h_i} \right) f'_i + \frac{1}{h_{i+1}} f'_{i+1} \right), \tag{21a}$$

where $h_{i-1} = x_i - x_{i-1}$, $h_i = x_{i+1} - x_i$, and the right-hand side can be evaluated once the first derivative at nodes has been computed from Eq. (9). For the last interval we can assume that the second derivative is the same at end-points, leading to

$$\frac{f_{n+1} - f_n}{h_n} = \frac{f'_n + f'_{n+1}}{2}. \tag{21b}$$

If we add the condition $f_1 = 0$, we obtain a tri-diagonal system of $n+1$ equations. The solution of this system provides the nodal values $f_i, i = 1\ldots n+1$, corresponding to the spline camberline with given nodal slope. We have implemented in our code this reconstruction procedure using the LSLTR subroutine from the IMSL library, as an alternative to Eq. (10). Note that the tri-diagonal system matrix is fixed, and only the right-hand side vector needs to be updated at each iteration. Moreover, solving this tridiagonal system of equations is more efficient than numerically computing the integral in Eq. (10).

The above spline representation for the camberline may display spurious oscillations for highly cambered blades. An alternative that sacrifices to some extent the accuracy is to employ a piecewise parabolic approximation for the camberline, thus integrating (9) as

$$f_i = f_{i-1} + (x_i - x_{i-1}) \frac{f'_i + f'_{i-1}}{2}, \text{ for } i = 2,\ldots,n+1 \text{ and with } f_1 = 0. \tag{22}$$

This is a second order scheme, equivalent to the trapezoidal rule of integration. The error for each subinterval of length $h = x_i - x_{i-1}$ is of order $O(h^3 f'')$, where the function's second derivative should be evaluated somewhere in the interval of integration. More accurate integration formulae can be used, but the computation becomes increasingly expensive as additional evaluations of f' are required within the interval of integration.

4. CONCLUSIONS

The paper presents a methodology for designing thin blade cascades, starting from a given distribution of tangential velocity from upstream to downstream. The blades are designed for a shock-free flow at leading edge. The authors develop and original numerical method for solving the nonlinear problem of finding the thin blade shape, and present two examples that clearly show how the blade shape is changing with the cascade spacing while the loading distribution and the overall flow deflection are kept constant. The convergence rate of the iterative algorithm for solving the non-linear integral equations is decreasing as the cascade spacing is increased. The analytical integration of main design equation (9), i.e. Eq. (10), can be replaced with a numerical integration or cubic spline reconstruction of the blade, without decreasing the overall accuracy of the results. However, the spline reconstruction of the blade shape may display spurious oscillations, therefore the numerical integration using a trapezoidal rule is more robust.

REFERENCES

1. ANTON, I., *Cavitația*, Editura Academiei Române, Bucureşti, 1985, vol. II, Cap. 7.
2. ANTON, Viorica, *Cercetări experimentale privind influența geometriei unor rețele de profile asupra caracteristicilor lor energetice şi cavitaționale*, Teza de doctorat, Institutul Politehnic "Traian Vuia" Timişoara, 1972.
3. ALTHAUS, D., WORTMANN, F.X., *StuttgarterProfilkatalog I. Experiemental Results from the Laminar Wind Tunnel of the Institut für Aero- und Gasdynamic de Universität Stuttgart*, Friedr. Vieweg & Sohn, Braunschweig/Wiesbaden, 1981.
4. CARTE, I.N., *Contribuții la studiul rețelelor de profile radial-axiale şi utilizarea lor în proiectarea rotorilor de turbine Francis*, Teza de doctorat, Institutul Politehnic "Traian Vuia" Timişoara, 1986.
5. GOSTELOW, J.P., *Cascade Aerodynamics*, Oxford, New York, Toronto, Pergamon Press, 1983.
6. GHEORGHIU, Monica, Studiul teoretic *şi experimental al caracteristicilor energetice ale rețelelor circulare de profile pentru aparate directoare de turbină*, Teza de doctorat, Institutul Politehnic "Traian Vuia" Timişoara, 1976.
7. HAWTHORNE, W.R., WANG, C., TAN, C.S., McCUNE, J.E., *Theory of Blade Design for Large Deflections: Part I – Two-Dimensional Cascade*, Journal of Engineering for Gas Turbines and Power, **106**, pp. 346-353, 1984.
8. HUGHES, J.R., The Finite *Element Method. Linear static and dynamic Finite Element Analysis*, Mineola, New York, Dover Publications, 2000 (reprint of *The Finite Element Method*, originally published by Prentice-Hall, 1987).
9. LEWIS, R.I., Turbomachinery Performance Analysis, Arnold, London, 1996, Ch. 2.
10. POPA, O., *Mişcări potențiale şi teoria hidrodinamicii rețelelor de profile*, Lito Institutul Politehnic "Traian Vuia" Timişoara, 1980.
11. von RIEGELS, F.W., *Aerodinamische Profile*, R. Oldenbourg, München, 1958.
12. ZANGENEH, M., *A Compressible Three-Dimensional Design Method for Radial and Mixed Flow Turbomachinery Blades*, International Journal of Numerical Methods in Fluids, **13**, pp. 599-624, 1991.
13. ZIDARU, Gh., Mişcări potențiale şi hidrodinamica rețelelor de profile, Editura Didactică şi Pedagogică, Bucureşti, 1981.

Redceived January 12, 2006